arXiv:1211.5649v1 [cond-mat.quant-gas] 24 Nov 2012

Direct observation of a Berezinskii-Kosterlitz-Thouless superfluid in an atomic gas

Jae-yoon Choi, Sang Won Seo, and Yong-il Shin*
Center for Subwavelength Optics and Department of Physics and Astronomy, Seoul National University, Seoul 151-747, Korea
(Dated: November 27, 2012)

Understanding the emerging mechanisms of superfluidity has been a central theme in many-body physics. In particular, the superfluid state in a two-dimensional (2D) system is intriguing because large thermal fluctuations prohibit the formation of long-range order [1, 2] and consequently the picture of Bose-Einstein condensation is not applicable to the phase transition. The Berezinskii-Kosterlitz-Thouless (BKT) theory [3, 4] provides a microscopic mechanism for the superfluid phase transition, where vortices with opposite circulation are paired below the critical temperature, establishing quasi-long-range phase coherence. While this mechanism has been tested experimentally [5–9], there has been no direct observation of thermal vortex pairs in a 2D superfluid. Here we report the observation of a BKT superfluid in a trapped quasi-2D atomic gas by measuring the spatial distribution of thermally activated vortices and revealing their pair correlations. The vortex population concentrates in the low-density superfluid region of the trapped sample and decreases gradually as the temperature is lowered, showing a crossover from a BKT phase to a Bose-Einstein condensate (BEC) with no thermal vortices. These observations clarify the nature of the superfluid state of a trapped 2D Bose gas.

The BKT mechanism represents a topological phase transition involving no spontaneous symmetry-breaking. The pairing of vortices is responsible for the emergence of a topological order for the low-temperature superfluid phase. Since vortex-antivortex pairs carry a zero net phase slip, the BKT superfluid can be described to be topologically identical to a state with a spatially uniform phase like a BEC on the large length scale compared to the vortex pair size, although it contains long-wavelength phase fluctuations due to thermal phonon excitations. Above the critical temperature, the topological character of the system disappears as free vortices, i.e. point defects, proliferate via unbinding of the vortex pairs, which is reflected in the decay behavior of phase coherence changing from algebraic to exponential. The BKT mechanism has been supported by experimental observations in many 2D systems [5–9]. However, a direct observation of thermally activated vortex pairs has been elusive.

Ultracold atomic gases in 2D geometry present a clean and well-controlled system for studying BKT physics. In particular, individual vortices can be detected in this system, providing interesting opportunities to directly test the microscopic nature of the BKT transition. Previous experimental studies of phase coherence [8, 10] and thermodynamic properties [11–13] indicated that a BKT-type transition occurs in a quasi-2D Bose gas trapped in a harmonic potential. Recently, superfluid behavior was demonstrated by measuring a critical velocity for friction-less motion of an obstacle [14]. In the present study, we measure the in-plane spatial distribution of thermally activated vortices in a quasi-2D Bose gas and reveal the vortex pairing from their spatial correlations. In addition, we observe that a vortex-free region emerges in the center of a trapped sample below a certain temperature, demonstrating crossover behavior of the superfluid state from a vortex-pair BKT phase to a vortex-free BEC phase [15, 16]. Our results clarify the nature of the superfluid state in an interacting 2D Bose gas trapped in a harmonic potential.

Our experiments are carried out with a quasi-2D Bose gas of ^{23}Na atoms in a pancake-shaped optical dipole trap [17]. A highly saturated thermal gas of ^{23}Na atoms in the $|F = 1, m_F = -1\rangle$ state is first generated in an optically plugged magnetic quadrupole trap, and transferred into an optical dipole trap that is formed by focusing a 1064 nm single laser beam. The final evaporative cooling is achieved by lowering the trap depth for 9 s. The trapping frequencies of the harmonic potential are $(\omega_x, \omega_y, \omega_z) = 2\pi \times (3.0, 3.9, 370)$ Hz, where the z-axis is along the direction of gravity. The dimensionless interaction strength $\tilde{g} = \sqrt{8\pi}a/l_z \simeq 0.013$, where a is the three-dimensional (3D) scattering length and $l_z = \sqrt{\hbar/m\omega_z}$ is the axial harmonic oscillator length (m is the atomic mass). For a typical sample of $N = 1.3 \times 10^6$ atoms, the zero-temperature chemical potential is estimated to be $\mu \simeq 0.7\hbar\omega_z$, where $\hbar$ is the Planck constant h divided by 2π, and thus, our sample constitutes a very weakly interacting quasi-2D Bose gas.

In this harmonic trap, the Bose-Einstein condensation temperature for a quasi-2D ideal gas of N atoms is $T_0 \approx 76$ nK (T_0 is calculated from the relation $N = \frac{k^2 T_0^2}{\hbar^2 \omega_x \omega_y} \sum_{\nu=0}^{\infty} \mathrm{Li}_2(e^{-\nu \frac{\hbar\omega_z}{kT_0}})$, considering thermal population in the tight direction, where $\mathrm{Li}_2(z)$ is the polylogarithm of order 2) and the BKT critical temperature is estimated in the mean-field theroy to be $T_c/T_0 \approx 0.99$ for our small $\tilde{g} = 0.013$ [18]. Below the superfluid phase transition, the sample shows a bimodal density distribution after time-of-flight expansion (Fig. 1a) [19]. We refer to the center part as the coherent part of the sample and

*Electronic address: yishin@snu.ac.kr

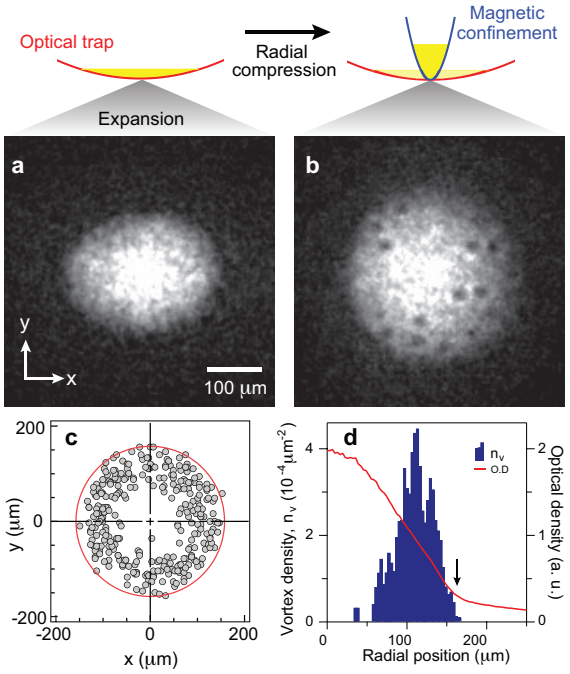

FIG. 1: Observation of thermally activated vortices. (a) Optical density image of a quasi-2D Bose gas, taken after a 17-ms time-of-flight expansion. Density ripples develop during the expansion due to phase fluctuations in the sample. (b) Image with applying a radial compression before the expansion. The radial compression is achieved by superposing a magnetic potential onto the sample in an optical trap. Quantized vortices are observed with density-depleted cores. (c) Positions of vortices with respect to the sample center recorded for 20 experimental realizations. The average number of vortices observed in a sample is $\bar{N}_v \approx 17$. (d) Radial profile of the vortex density $n_v(r)$. The red solid line displays the atom density profile $n(r)$ of the sample, showing a bimodal distribution. The center part is refered to as the coheret part of the sample and its boundary is indicated by an arrow in (d) and a red solid line in (c). The data are acquired for $N = 1.6(2) \times 10^6$ atoms at $T = 50(6)$ nK.

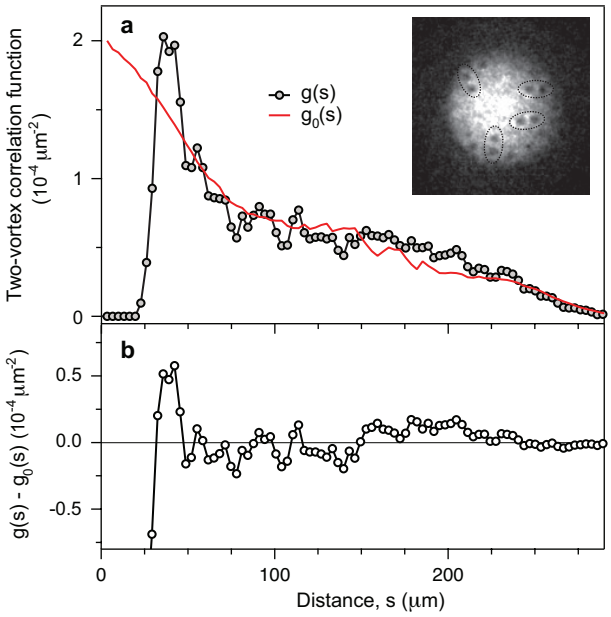

FIG. 2: Pair correlations of vortices. (a) Two-vortex spatial correlation function $g(s)$, obtained from 20 images for the experimental condition in Fig. 1. The red solid line represents the correlation function $g_0(s)$ for an uncorrelated distribution with the same vortex density profile $n_v(r)$ in Fig. 1c. The inset displays Fig. 1b with guide lines for pairs of vortices whose separation is less than 30 μm. (b) The difference $g(s) - g_0(s)$ shows oscillatory behavior with a noticeable enhancement at $s \sim 35$ μm.

determine the sample temperature T from the gaussian width of the outer low-density thermal wing.

The conventional method for detecting quantized vortices is observing density-depleted vortex cores after releasing the trap [20]. Because the vortex core size $\xi \propto n^{-1/2} \propto R^{3/2}$, where n is the atom density and R is the sample size, the vortex core expands generally faster than the sample in a 3D case [21], facilitating its detection. For a 2D Bose gas, however, this method is not adequate because of the initial fast expansion along the tight confining direction which reduces atom interaction effects so rapidly that the vortex core structure is not maintained during the subsequent evolution. Furthermore, phase fluctuations present in the 2D sample evolve into density modulations [17], making the detection of individual vortices more difficult.

To improve the visibility of the vortex cores, we apply a radial compression to the sample before expansion. The compression transforms the 2D sample into an oblate 3D sample with $\mu/\hbar\omega_z > 1$, restoring the favorable condition for the vortex detection [21]. Furthermore, in the compressed sample, thermal relaxation of phonon excitations will proceed because of the change in the dimensionality of the sample. Vortices may also decay, but the effective 2D geometry in terms of vortex relaxation can be preserved for a moderate compression, suppressing Kelvin mode excitations on a vortex line [22].

In our experiment, the radial compression is achieved by superposing a quadrupole magnetic potential onto the sample. The axial axis of the magnetic quadrupole field is aligned with that of the sample. We control the field gradient and the position of the zero-field point to increase the trapping frequencies at the center of the hybrid trap almost linearly to $\omega_{x,y} = 2\pi \times 39$ Hz for 0.4 s, and let the sample relax for 0.2 s that corresponds to about 10 collision times. There was no significant collective oscillation of the sample, and the atom number fraction for the cohrent part was reduced by about 7% in this process. The chemical potential of the compressed sample is estimated to be $\mu/\hbar w_z > 5$, reaching a 3D regime. This was confirmed by making a condensate in the tight trap and observing no phase fluctuations [17]. To magnify vortex cores, we employ a two-step expansion: First, we suddenly turn off only the magnetic potential to make the sample expand radially for 6 ms in the optical trap, and

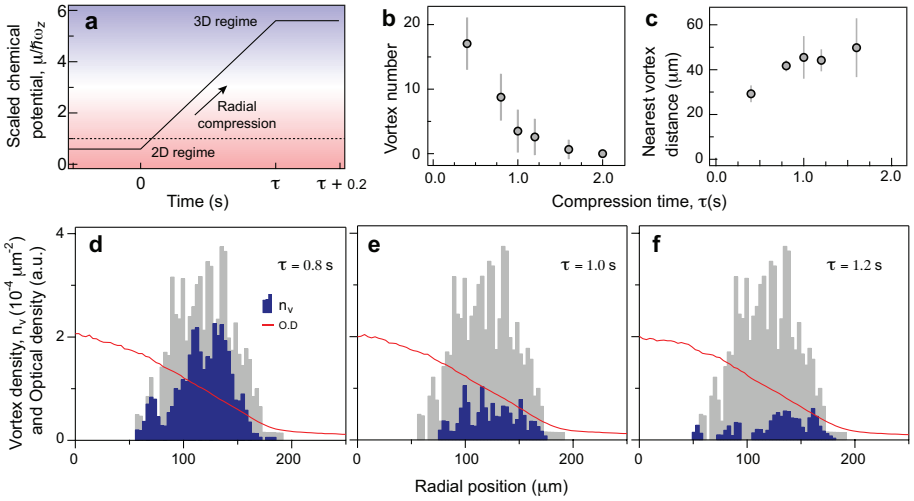

FIG. 3: Compression time dependence of the vortex distribution. (a) Evolution of the scaled chemical potential $\mu/\hbar\omega_z$ in the radial compression process. (b) Vortex number N_v and (c) nearest vortex distance d_m versus compression time τ. (d, e, f) Radial profiles of the vortex density for various compression times. The vortex density profile for $\tau = 0.4$ s is displayed in the background and the red solid lines show the atom density profiles. These data are acquired for $N = 1.8(2) \times 10^6$ atoms at $T = 46(6)$ nK. Error bars indicate standard deviation.

then switch off the optical trap for further magnification. It is not clear why the in-trap expansion could enhance the contrast of vortex cores, which is not an exact 2D expansion. Finally, we take an absorption image along the axial direction after additional 9 ms of time-of-flight expansion to measure the in-plane density distribution of the sample.

Using this procedure, we observe thermally excited vortices with clear density-depleted cores (Fig. 1b). This indicates the existence of vortex-antivortex pair excitations because the direct generation of single vortices is forbidden. The core size is measured to be $\xi_v \approx 8$ μm, allowing by-hand locating of the vortices that gives the vortex distribution $\rho_v(\vec{r}) = \Sigma_{i=1}^{N_v} \delta(\vec{r} - \vec{r}_i)$, where N_v is the number of voritces and $\vec{r}_i$ is the position of the i-th vortex with respect to the center of the sample. At $T \approx 50$ nK, the average vortex number is about 17 and vortices mainly appear in the outer region of the coherent part. There is no azimuthal dependence of the vortex distribution (Fig. 1c) and the radial profile of the vortex density $n_v(r)$ is obtained by azimuthally averaging the averaged $\rho_v(\vec{r})$ for the same experiments (Fig. 1d). The vortex region ($n_v > 0$) reaches the boundary of the coherent part, implying the existence of a vortex-driven phase transition. Density modulations suggestive of vortex cores are often observed at the boundary, but not included in the vortex counting.

One notable feature in the vortex distribution is frequent appearance of a pair of vortices that are closely located to each other but well separated from the others (Fig. 2 inset). We measure the distance from every vortex to its nearest vortex and find its average value to be $d_m \approx 4\xi_v$. A more quantitative study of the pair correlations is performed with the two-vortex spatial correlation function:

$$g(s) = \frac{1}{\pi s N_v (N_v - 1)} \sum_{i>j} \delta(s - r_{ij}) \qquad (1)$$

where $r_{ij} = |\vec{r}_i - \vec{r}_j|$. This function displays the probability of finding a vortex at distance s from another vortex, containing rich information about vortex interactions. We determine $g(s)$ as the average of the pair correlation functions individually obtained from images for the same experiments (Fig. 2a). In order to see vortex interaction effects, we compare $g(s)$ to the pair correlation function for an uncorrelated vortex distribution having the same vortex density profile $n_v(r)$: $g_0(s) = \int dr d\theta\ r n_v(r) n_v(r') / [\int dr 2\pi r n_v(r)]^2$ where $r' = \sqrt{r^2 + 2rs\cos\theta + s^2}$. The difference $g(s) - g_0(s)$ shows a noticeable enhancement around $s \sim d_m$ and small oscillatory behavior at large s, clearly indicating that there are attractive interactions between closely located vortices. The complete suppression at $s < 3\xi_v$ is attributed to the annhilations of tightly bound vortex pairs during the compression and expansion process. When we slowly compress the sample, the vortex number N_v rapidly reduces over 1 s, but d_m increases more slowly than $N_v^{-1/2}$ (Fig. 3b and c).

The pairing feature in $g(s)$ becomes more pronounced at lower temperatures (Fig. 4i-k), which we ascribe to the temperature dependence of the characteristic size of vortex pairs. The thermal excitation probability p of a vortex-antivortex pair is estimated from the associated free energy $F = E - TS$ as $p \propto e^{-F/kT}$ where k is the Boltzmann constant. The excitation energy E of a vortex pair of size d is $\sim \frac{h^2}{2\pi m} n_s \ln(d/\xi)$ where n_s is the superfluid density [15]. In a superfluid region of size R, the number of distinguishable microstates

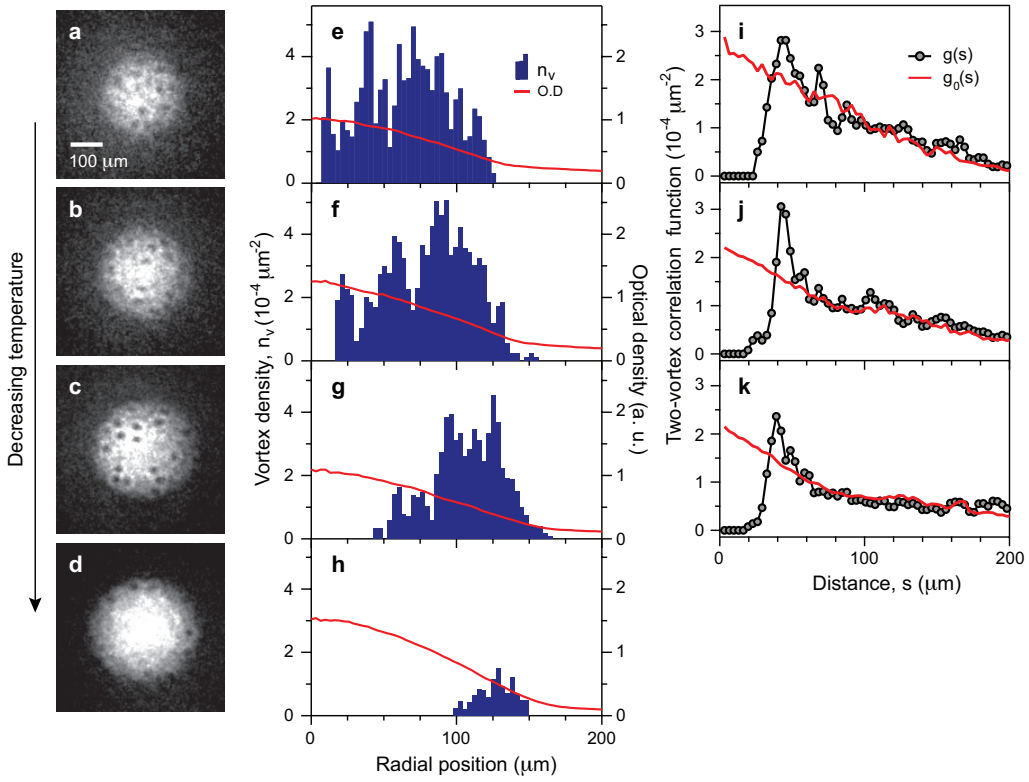

FIG. 4: Thermal excitations of vortices in a trapped 2D Bose gas. The left column (a-d) displays examples of vortex images for various temperatures. The experimental parameters and the votex number are $(N, T, N_v) = (1.5(2) \times 10^6, 67(12)$ nK, $13(4))$ for (a), $(1.4(3) \times 10^6, 56(6)$ nK, $16(4))$ for (b), $(1.3(1) \times 10^6, 48(8)$ nK, $15(5))$ for (c), and $(1.0(3) \times 10^6, 23(4)$ nK, $2(4))$ for (d). The middle column (e-h) and the right column (i-k) show the radial profiles of the vortex density $n_v(r)$ and the pair correlation functions $g(s)$, respectively, for the experimental conditions in (a-d). The data are obtained from at least 12 images for each condition. $g(s)$ for the lowest temperature (d) is not reliably determined due to the small vortex number. The red solid lines in (e-h) and (i-k) represents $n(r)$ and $g_0(s)$, respectively.

for the vortex pair is $\sim \frac{R^2}{\xi^2}\frac{\pi d}{\xi}$, where the first and the second terms correspond respectively to the position of a single vortex in the region and the relative orientation of two vortices with separation d, which gives the entropy $S = k\ln(\pi d R^2/\xi^3)$. In this estimation, $p \propto \frac{R^2}{\xi^2}(d/\xi)^{-(n_s\lambda^2-1)}$ where $\lambda = h/\sqrt{2\pi mkT}$ is the thermal wavelength. Therefore, tightly bound pairs are relatively more populated at lower temperatures, leading to more enhancement at smaller s in the pair correlation function. These obsevations provide conclusive evidence for the pairing of vortices in the superfluid phase in a quasi-2D Bose gas.

Figure 4e-h display the vortex density profiles $n_v(r)$ for various temperatures. Because the thermal excitation probability is exponentially suppressed by $n_s\lambda^2$, $n_v(r)$ reflects the spatial distribution of the superfluid density $n_s(r)$. At high temperature near the critical point, vortex excitations prevail over the whole coherent part, and as temperature is lowered, a vortex-free region starts emerging in the center of the sample, pushing vortices outwards. At $T \approx 30$ nK, only a few vortices appear near the boundary of the coherent part. The emergence of a vortex-free region indicates the change in the microscopic nature of the superfluid phase. This represents a crossover from a BKT phase to a BEC phase, continously suppressing the vortex-pair excitations. In a finite-size 2D system, forming a BEC is expected at finite temperature when the coherence length of the superfluid becomes comparable to the spatial size of the system [15, 16].

The BKT theory for a homogeneous system predicts spontaneous unbinding of vortex pairs and a sudden drop of the superfluid density at the critical point [23]. These would be revealed in our experiments as a rapid change in the pair correlations or/and sharp behavior of the outer boundary of the vortex region. However, these are not observed in our experiments. This might be due to the limited sensitivity of our detection method in the critical region and possibly, drifting of vortices out of the coherent part during the compression process. On the other hand, the distinction between vortex pairs and free vorices is not clear in a finite system and the behavior of vortices might be expected to be continuous over the critical point [8].

We summarize our results in Figure 5 with a phase diagram of a 2D Bose gas in a harmonic potential. The in-situ critical radius R_c for the superfluid-to-normal phase

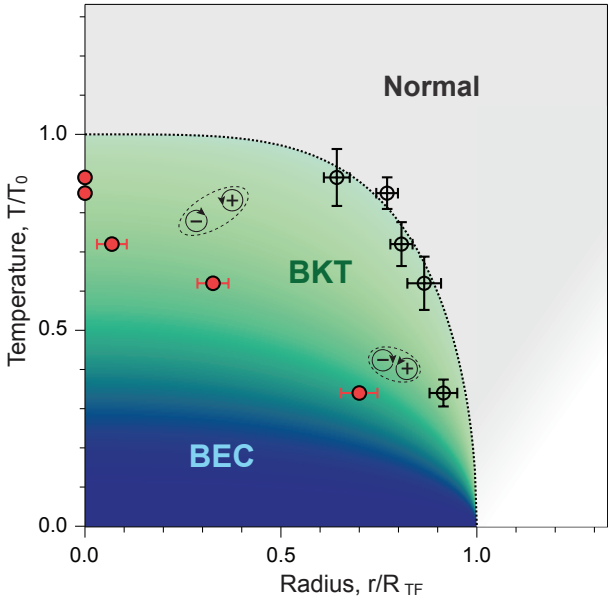

FIG. 5: BKT-BEC crossover. The phase diagram of a 2D Bose gas trapped in a harmonic potential is depicted in the plane of $r/R_{\rm TF}$ and T/T_0. $R_{\rm TF}$ is the 2D Thomas-Fermi radius, and T_0 is the BEC temperature for a quasi-2D ideal gas in the harmonic potential. A BKT superfluid phase containing vortex-pair excitations emerges below a critical temperature. The in-situ critical radius R_c for the superfluid-to-normal phase transition are indicated by open circles, estimated from the radius of the coherent part, including the time-of-flight expansion factor. The red dashed line is $r/R_{\rm TF} = \sqrt{1-(T/T_0)^{4.2}}$ as a guide for the critical line. As the temperature is decreased, thermal excitations of vortex pairs are suppressed, preferentially in the center region of high superfluid density, leading to the emergence of a BEC phase at low temperature. Red solid circles represent the inner radii R_v of the vortex region ($n_v > 0$), determined with the assumption that R_v/R_c is preserved during the compression and expansion process. Error bars indicate standard deviation.

transition is determined from the radius of the coherent part in the x-direction measured in images taken without the compression process as Fig. 1a, including the expansion factor for 17-ms time-of-flight that was measured to be 1.03(1) from a fit of $R_c(1-\alpha t^2)$ to the radii of the coherent part for various time-of-flight $t = 10 \sim 25$ ms. The 2D Thomas-Fermi radius $R_{\rm TF} = (\frac{4\hbar^2 N\tilde{g}\omega_y}{\pi m^2\omega_x^3})^{1/4}$ for the x-direction. The vortex region is marked as a BKT phase, where the inner radius R_v is determined from a hyperbolic-tangent fit to the inner region of $n_v(r)$ with a threshold value of 6×10^{-5} μm^{-2}. Here, we assume that the relative radial position R_v/R_c is preserved in the radial compression and expansion process. Because a vortex pair carries a linear momentum of h/d, the vortex region might be broadened by diffusion during the compression. However, we observed that the inner radius R_v of the vortex region does not change significantly for longer compression times (Fig. 3d-f), probably because it is energetically unfavorable for vortices to intrude into the center region with high superfluid density. In recent theoretical studies [24, 25], the critical temperature for the emergence of a BEC phase was calculated as a point when the thermal excitation probability of a vortex pair becomes of order unity. Our results show qualitative agreement with the predictions, but their direct comparison is limited because the vortex detection efficiency of our imaging method is not determined.

In conclusion, we have observed thermally activated vortex pairs in the superfluid phase of a 2D Bose gas trapped in a harmonic potential. This provides the clear confirmation of BKT superfluidity in the systems. The experimental study of 2D superfluidity has been recently extended to ultracold atom systems including disorder potentials [26] and Fermi gases [27], and new research directions with spin degrees of freedom [28] and in a dynamic transition regime [29] have been theoretically proposed. The vortex detection method developed in this work will be an important tool to probe the microscopic properties of these systems. Integrated with an inteferometric technique [10, 30], this method might be upgraded to be sensitive to the sign of a vortex.

We thank W. J. Kwon for experimental assistance. This work was supported by the NRF of Korea funded by MEST (Grants No. 2010- 0010172, No. 2011-0017527, No. 2008-0062257, and No. WCU-R32-10045). We acknowledge support from the Global PhD Fellowship (J.C.), the Kwanjeong Scholarship (S.W.S.), and the T.J. Park Science Fellowship (Y.S.).

[1] Mermin, N. D. & Wagner, H. Absence of ferromagnetism or antiferromagnetism in one- or two-dimensional isotropic Heisenberg models. *Phys. Rev. Lett.* **17**, 1133–1136 (1966).
[2] Hohenberg, P. C. Existence of long-range order in one and two dimensions. *Phys. Rev.* **158**, 383–386 (1967).
[3] Berezinskii, V. L. Destruction of long-range order in one-dimensional and two-dimensional systems possessing a continuous symmetry group. II. Quantum systems. *Sov. Phys. JETP* **34**, 610–616 (1972).
[4] Kosterlitz, J. M. & Thouless, D. J. Ordering, metastability and phase transitions in two-dimensional systems. *J. Phys. C* **6**, 1181–1203 (1973).
[5] Bishop, D. J. & Reppy, J. D. Study of the superfluid transition in two-simensional ^{4}He films. *Phys. Rev. Lett.* **40**, 1727–1730 (1978).
[6] Resnick, D. J., Garland, J. C., Boyd, J. T., Shoemaker, S. & Newrock, R. S. Kosterlitz-Thouless transition in proximity-coupled superconducting arrays. *Phys. Rev. Lett.* **47**, 1542–1545 (1981).
[7] Safonov, A. I., Vasilyev, S. A., Yasnikov, I. S., Lukashevich, I. I & Jaakkola, S. Observation of quasicondensate in two-dimensional atomic hydrogen. *Phys. Rev. Lett.* **81**, 4545–4548 (1998).

[8] Hadzibabic, Z., Krüger, P., Cheneau, M., Battelier, B. & Dalibard, J. Berezinskii-Kosterlitz-Thouless crossover in a trapped atomic gas. *Nature* **441**, 1118–1121 (2006).

[9] Schweikhard, V., Tung. S., & Cornell, E. A. Vortex proliferation in the Berezinskii-Kosterlitz-Thouless regime on a two-dimensional lattice of Bose-Einstein condensates. *Phys. Rev. Lett* **99**, 030401 (2007).

[10] Cladé, P., Ryu, C., Ramanathan, A., Helmerson, K & Phillips, W. D. Observation of a 2D Bose gas: from thermal to quasicondensate to superfluid. *Phys. Rev. Lett* **102**, 170401 (2009).

[11] Tung, S., Lamporesi, G., Lobser, D., Xia, L. & Cornell, E. A. Observation of the pre- superfluid regime in a two-dimensional Bose gas. *Phys. Rev. Lett* **105**, 230408 (2010).

[12] Hung, C. L., Zhang, X., Gemelke, N. & Chin, C. Observation of scale invariance and universality in two-dimensional Bose gases. *Nature* **470**, 236–239 (2011).

[13] Yefsah, T., Desbuquois, R., Chomaz,L., Günter K. J. & Dalibard, J. Exploring the thermodynamics of a two-dimensional Bose gas. *Phys. Rev. Lett* **107**, 130401 (2011).

[14] Desbuquois, R. *et al.* Superfluid behaviour of a two-dimensional Bose gas. *Nature Phys.* **8**, 645–648 (2012).

[15] Simula, T. P., Lee, M. D. & Hutchinson, D. A. W. Transition from the Bose-Einstein condensate to the Berezinskii-Kosterlitz-Thouless phase. *Philos. Mag. Lett.* **85**, 395–403 (2005).

[16] Esslinger, T. & Blatter, G. Atomic gas in flatland. *Nature* **441**, 1053–1054 (2006).

[17] Choi, J., Seo, S. W., Kwon, W. J. & Shin, Y. Probing phase fluctuations in a 2D degenerate Bose gas by free expansion. *Phys. Rev. Lett.* **109**, 125301 (2012).

[18] Holzmann, H., Chevallier, M. & Krauth W., Semiclassical theory of the quasi-two-dimensional trapped Bose gas. *Europhys. Lett.* **82**, 30001 (2008).

[19] Krüger, P., Hadzibabic, Z. & Dalibard, J. Critical point of an interacting two-dimensional atomic Bose gas. *Phys. Rev. Lett.* **99**, 040402 (2007).

[20] Madison, K. W., Chevy, F., Wohlleben, W. & Dalibard, J. Vortex formation in a stirred Bose-Einstein condensate. *Phys. Rev. Lett.* **84**, 806–809 (2000).

[21] Dalfovo, F. & Modugno, M. Free expansion of Bose-Einstein condensates with quantized vortices. *Phys. Rev. A* **61**, 023605 (2000).

[22] Rooney, S. J., Blakie, P. B., Anderson, B. P. & Bradley, A. S. Suppression of Kelvon-induced decay of quantized vortices in oblate Bose-Einstein condensates. *Phys. Rev. A* **84**, 023637 (2011).

[23] Nelson, D. R. & Kosterlitz, J. M. Universal jump in the superfluid density of two-dimensional superfluids. *Phys. Rev. Lett.* **39**, 1201–1205 (1977).

[24] Simula, T. P. & Blakie, P. B. Thermal activation of vortex-antivortex pairs in quasi-two-dimensional Bose-Einstein condensates. *Phys. Rev. Lett.* **96**, 020404 (2006).

[25] Schumayer, D. & Hutchinson, D. A. W. Thermodynamically activated vortex-dipole formation in a two-dimensional Bose-Einstein condensate. *Phys. Rev. A* **75**, 015601 (2007).

[26] Allard, B. *et al.* Effect of disorder close to the superfluid transition in a two-dimensional Bose gas. *Phys. Rev. A.* **85**, 033602 (2012).

[27] Feld, M., Fröhlich, B., Vogt, E., Koschorreck, M. & Köhl, M. Observation of a pairing pseudogap in a two-dimensional Fermi gas. *Nature* **480**, 75–78 (2011).

[28] James, A. J. A. & Lamacraft, A. Phase diagram of two-dimensional polar condensates in a magnetic field. *Phys. Rev. Lett.* **106**, 140402 (2011).

[29] Mathey, L., Günter, K J., Dalibard, J. & Polkovnikov, A. Dynamic Kosterlitz-Thouless transition in 2D Bose mixtures of ultra-cold atoms. arXiv:1112.1204 (2011).

[30] Roumpos, G. *et al.* Single vortex-antivortex pair in an exciton-polariton condensate. *Nature Phys.* **7**, 129–133 (2011).